IEEE Access
Multidisciplinary | Rapid Review | Open Access Journal

Received February 16, 2020, accepted March 9, 2020, date of publication March 17, 2020, date of current version March 26, 2020.

Digital Object Identifier 10.1109/ACCESS.2020.2981576

Numeric Study of Novel Compact Polarimeter for Full-Stokes Polarization Imaging Without Micro-Polarizer Array

NAITING GU[1,2], DUO XU[1,2,3], LINHAI HUANG[1,2], AND CHANGHUI RAO[1,2]

[1]Institute of Optics and Electronics, Chinese Academy of Sciences, Chengdu 610209, China
[2]The Key Laboratory on Adaptive Optics, Chinese Academy of Sciences, Chengdu 610209, China
[3]School of Optoelectronic Science and Engineering, University of Electronic Science and Technology of China, Chengdu 610000, China

Corresponding authors: Naiting Gu (gnt7328@163.com) and Linhai Huang (hlhjs@163.com)

This work was supported in part by the National Natural Science Foundation of China under Grant 11727805 and Grant 61905252, and in part by the Youth Innovation Promotion Association, Chinese Academy of Science, under Grant 2018412.

ABSTRACT This paper proposed a novel polarimeter for full-Stokes polarization imaging without using any kind of micro-polarizer array. The key components of the polarimeter are two grooved birefringent crystal plates with deviate fast axis, which are called Binary Birefringent Crystals (BBCs) in this paper. Mounting the jointed BBCs in the focal plane of an imaging detector, we manage to obtain the four components of Stokes vector simultaneously through the method proposed in this paper. We demonstrate the basic principle of the proposed polarimeter and verify it through numerical analysis. And one of the best-optimized configurations for the polarimeter is also presented. The proposed polarimeter is simultaneous, compact, easier in fabrication and capable of full-stokes polarization imaging. It is expected to be of potential use in a variety of applications.

INDEX TERMS (110.5405) polarimetric imaging, (110.0110) imaging system, (120.0120) instrumentation, measurement, and metrology.

I. INTRODUCTION

Polarization imaging technologies are capable of recording light polarization of a scene, which implies certain characteristics of the objects, such as surface features, shapes, shadows, and roughness. It improves the target recognition in complicate environment and provides valuable information for target detection [1], biomedical imaging [2], [3], material characterization [4], environmental monitoring [5], astronomy observation [6] and remote sensing [7]. The Stokes vector is generally used to describe the state of polarization (SOP) of incident light, and it can provide more information about reflecting objects than traditional intensity-based cameras. The most traditional polarization imaging technique adopt temporal polarization modulation and time-sequential data acquisition using rotating elements [8], photoelastic modulators [9], electro-optical modulators [10], liquid crystal retarders [11], or binary polarization rotators [12]. Such temporal polarimeters need at least four measurements at different times, which require a stationary scene in order to avoid temporal blur. To eliminate these disadvantages, two kinds of polarimeters, i.e. division of amplitude [13] and division of aperture [14], were proposed for simultaneous polarization imaging which divide the beam under test into several sub-beams and capture multiple images simultaneously by using independent cameras or a single camera. However, the problem converts into spatial registration of polarization images due to separate optical paths. Besides, large and complex optical and mechanical configurations also limit the applications of these kinds of designs. In contrast of the mentioned designs above, the polarimeter of division of focal plane (DoFP) [15–[20], which utilizes four independent micro-polarimeters to obtain full Stokes vector, is a promising avenue with significant advantages of low cost, compact size, light weight, and stable performance. The early DoFP polarimeters were realized with micro-polarizer arrays (MPAs), such as aluminum nanowire MPA [18], rubbed polyvinyl-alcohol (PVA) MPA [19] and liquid crystal polymer (LCP) MPA [20]. One limitation of this kind of DoFP polarimeters is that the micro-polarizer is hard to make and align. Meanwhile they are only capable of measuring the linear Stokes components.

The associate editor coordinating the review of this manuscript and approving it for publication was Chaitanya U. Kshirsagar.

Full-stokes DoFP polarimeters were first presented with patterned LCP polarizers and retarders [21], [22]. However, the accuracy was not sufficiently high due to certain aspects of their designs [23]. Moreover, this approach was limited in a few areas of researches and applications due to the complicated process in manufacturing and unstable property of LCP polarizers and retarders [24], [25].

In this paper, a novel DoFP polarimeter for full-Stokes polarization imaging is proposed without using any kinds of MPA, which will make the fabrication of DoFP polarimeter much easier. The core components of the proposed novel polarimeter are a piece of the jointed Binary Birefringent Crystals (BBCs), a thin polarizer and a camera, which are mounted in focal plane of an imaging detector. Different from current polarimeters, the proposed polarimeter takes advantages of different retardances with different thickness of the birefringent crystal and derives the state of polarization of the incident beam from the camera image. It is expected to be of potential use in a variety of applications. This paper is organized as follows. In section II, we will introduce the concept and theory of the proposed polarimeter; in section III, we will validate the performance of the proposed polarimeter by numeric analysis and tolerance analysis; finally, a conclusion and discussion will be made in section IV.

II. CONCEPT AND THEORY

A basic polarimeter for polarization imaging is generally composed of three fundamental components including imaging lens, polarization modulator and photo camera. Fig. 1 shows the schematic layout of a polarization imaging system, which consists of imaging lens and the proposed polarimeter. Different from a general imaging system, a jointed Binary Birefringent Crystals (BBCs) and a thin polarizer are mounted in the focal plane of an imaging detector. The BBCs are the main components of the polarimeter. They are two grooved birefringent crystal plates with deviate fast axis, as shown in Fig. 2. Grooves with equal width to the bulges are etched into the birefringent crystal plates. The widths and the depths of the grooves and the fast axis angle

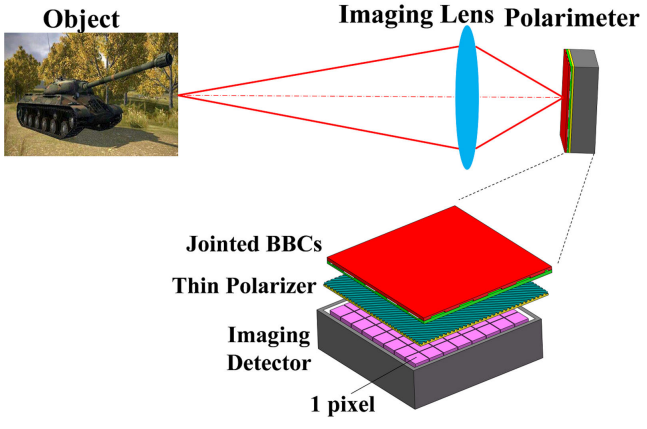

FIGURE 1. Schematic diagram of the proposed polarimeter with a piece of jointed BBCs.

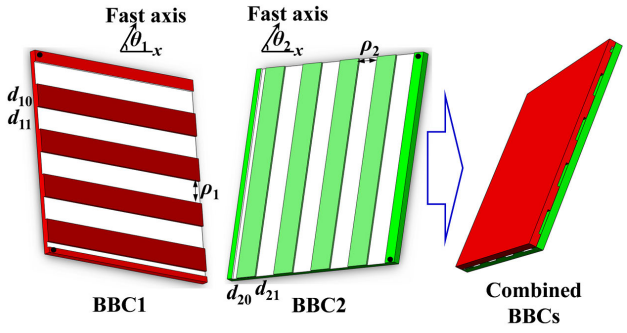

FIGURE 2. Schematic diagram of the jointed BBCs. $\theta_{1/2}$, angel of the fast axis of BBC1/2 relative to x axis. $\rho_{1/2}$, groove width of BBC1/2. d_{10}/d_{20}, thickness of the BBCs. d_{11}/d_{21}, depth of the grooves. Four black dots, jointing indicator points.

for these two BBCs can be used to fit the chosen imaging detector and to optimize the performance of polarization imaging for different applications. The BBCs are jointed on the edge by photosensitive glue with the grooves perpendicular to each other, forming periodical groups of four adjacent retarder pairs with different polarization modulation properties. Mounting the jointed BBCs together with thin polarizer in the focal plane of an imaging detector enables four independent and simultaneous polarization measurements.

The polarization retardance of each rectangle depends on the thickness of the BBCs (i.e. d_{10} and d_{20}), the depth of the grooves (i.e. d_{11} and d_{21}), the type of birefringent crystal, and the angles from the fast axes of BBCs to horizontal direction (i.e. x axis). The rectangles formed by the jointed BBCs should have the same size as the pixel of the imaging detector, which means the width of the grooves of the BBCs (i.e. ρ_1 and ρ_2 respectively) should match the width and length of the pixel of the imaging detector respectively. And periodical rectangles should align to pixels of the imaging detector one by one during integration process.

The imaging detector measures the light intensity passing the four rectangles of a group simultaneously. The values of the Stokes vector components of the incident light can be calculated from the measurements. The polarization retardances of the light passing the BBCs can be presented as

$$\delta_{ij} = \mathrm{mod}\left[\frac{2\pi}{\lambda}(n_{oi} - n_{ei})d_{ij}, 2\pi\right], \quad i = 1, 2;\ j = 0, 1 \quad (1)$$

where mod $[\cdot]$ is a remainder operator, which gets the remainder from the first item divided by 2π. λ is the wavelength of the incident light. i is the sequence number of BBC$_i$. j marks the bulges and grooves (0 for bulges, 1 for grooves). n_{oi} and n_{ei} are the refractive index of BBC$_i$ for o-light and e-light respectively. For negative birefringent crystal, the n_{oi} is larger than n_{ei}, and its polarization retardance δ_{ij} is negative. Similarly, the polarization retardance δ_{ij} is positive for positive birefringent crystal. To avoid unexpected additional modulation between adjacent points, a telecentric imaging lens is suggested.

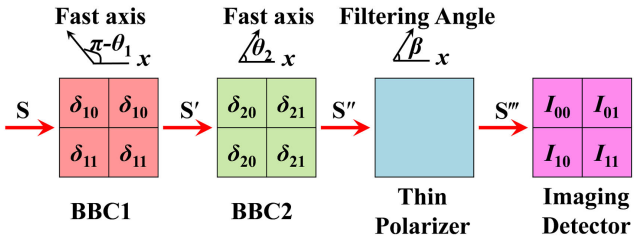

FIGURE 3. Polarization modulation process of the proposed polarimeter. β, the filtering angle of the thin polarizer. I_{mn}, light intensity at four adjacent pixels of detector when $m = 0,1$ and $n = 0,1$. (S, S′, S″, S‴), the original Stokes vector of the incident light, and the ones passing BBC1, BBC2 and the thin polarizer.

Suppose the Stokes vector of the incident light is $\mathrm{S} = (S_0, S_1, S_2, S_3)^{\mathrm{T}}$, and the ones passing BBC1, BBC2 and the thin polarizer are $\mathrm{S}' = (S_0', S_1', S_2', S_3')^{\mathrm{T}}$, $\mathrm{S}'' = (S_0'', S_1'', S_2'', S_3'')^{\mathrm{T}}$ and $\mathrm{S}''' = (S_0''', S_1''', S_2''', S_3''')^{\mathrm{T}}$ respectively, as shown in Fig. 3. Take four adjacent pixels of a group for example, and the position of the pixels are marked by row ($m = 0, 1$) and column ($n = 0, 1$). Then S''' can be expressed as

$$\mathbf{S}'''_{m,n} = \mathbf{M}_P(\beta) \cdot \mathbf{M}_{BBC2}(\theta_2, \delta_{2n}) \cdot \mathbf{M}_{BBC1}(\pi - \theta_1, \delta_{1m})\mathbf{S} \tag{2}$$

where $\mathbf{M}_P(\beta)$, $\mathbf{M}_{BBC2}(\theta_2, \delta_{2n})$ and $\mathbf{M}_{BBC1}(\pi - \theta_1, \delta_{1m})$ present the Mueller matrixes of the thin polarizer, BBC2 and BBC1 at pixel (m, n) respectively, and they can be written as (3)–(5) shown at the bottom of the next page.

Thus the equation (2) can be rewritten as

$$\begin{bmatrix} S'''_{0,(m,n)} \\ S'''_{1,(m,n)} \\ S'''_{2,(m,n)} \\ S'''_{3,(m,n)} \end{bmatrix} = \mathbf{M}^{(m,n)} \begin{bmatrix} S_0 \\ S_1 \\ S_2 \\ S_3 \end{bmatrix} = \begin{bmatrix} M_{11}^{(m,n)} & M_{12}^{(m,n)} & M_{13}^{(m,n)} & M_{14}^{(m,n)} \\ M_{21}^{(m,n)} & M_{22}^{(m,n)} & M_{23}^{(m,n)} & M_{24}^{(m,n)} \\ M_{31}^{(m,n)} & M_{32}^{(m,n)} & M_{33}^{(m,n)} & M_{34}^{(m,n)} \\ M_{41}^{(m,n)} & M_{42}^{(m,n)} & M_{43}^{(m,n)} & M_{44}^{(m,n)} \end{bmatrix} \begin{bmatrix} S_0 \\ S_1 \\ S_2 \\ S_3 \end{bmatrix} \tag{6}$$

where $\boldsymbol{M}^{(\mathbf{m},\mathbf{n})}$ is the Mueller matrix for the whole polarization modulation process, and can be presented as

$$\mathbf{M}^{(m,n)} = \mathbf{M}_P(\beta) \cdot \mathbf{M}_{BBC2}(\theta_2, \delta_{2n}) \cdot \mathbf{M}_{BBC1}(\pi - \theta_1, \delta_{1m}) \tag{7}$$

Only light intensity (i.e. the first component of $\mathbf{S}'''$) can be measured by the imaging detector. So the first line of equation (6) for four adjacent pixels can be presented as

$$\begin{bmatrix} I_{00} \\ I_{01} \\ I_{10} \\ I_{11} \end{bmatrix} = \begin{bmatrix} S'''_{0,(0,0)} \\ S'''_{0,(0,1)} \\ S'''_{0,(1,0)} \\ S'''_{0,(1,1)} \end{bmatrix} = \begin{bmatrix} M_{11}^{(0,0)} & M_{12}^{(0,0)} & M_{13}^{(0,0)} & M_{14}^{(0,0)} \\ M_{11}^{(0,1)} & M_{12}^{(0,1)} & M_{13}^{(0,1)} & M_{14}^{(0,1)} \\ M_{11}^{(1,0)} & M_{12}^{(1,0)} & M_{13}^{(1,0)} & M_{14}^{(1,0)} \\ M_{11}^{(1,1)} & M_{12}^{(1,1)} & M_{13}^{(1,1)} & M_{14}^{(1,1)} \end{bmatrix} \begin{bmatrix} S_0 \\ S_1 \\ S_2 \\ S_3 \end{bmatrix} \tag{8}$$

Put (3)-(5) into (6), the first-row elements of the Mueller matrix at position (m, n) can be presented as

$$\begin{aligned}
M_{11}^{(m,n)} &= 0.5 \\
M_{12}^{(m,n)} &= 0.5[\cos 2\theta_2 \cos 2(\beta-\theta_2) - \sin 2\theta_2 \sin 2(\beta-\theta_2) \cos \delta_{2n}] \\
&\quad \left(\cos^2 2\theta_1 + \sin^2 2\theta_1 \cos \delta_{1m}\right) \\
&\quad - 0.5[\sin 2\theta_2 \cos 2(\beta-\theta_2) + \cos 2\theta_2 \sin 2(\beta-\theta_2) \cos \delta_{2n}] \\
&\quad \sin 2\theta_1 \cos 2\theta_1 (1 - \cos \delta_{1m}) \\
&\quad - 0.5 \sin 2(\beta - \theta_2) \sin \delta_{2n} \sin 2\theta_1 \sin \delta_{1m} \\
M_{13}^{(m,n)} &= -0.5[\cos 2\theta_2 \cos 2(\beta-\theta_2) - \sin 2\theta_2 \sin 2(\beta-\theta_2) \cos \delta_{2n}] \\
&\quad \sin 2\theta_1 \cos 2\theta_1 (1 - \cos \delta_{1m}) \\
&\quad + 0.5[\sin 2\theta_2 \cos 2(\beta-\theta_2) + \cos 2\theta_2 \sin 2(\beta-\theta_2) \cos \delta_{2n}] \\
&\quad \left(\sin^2 2\theta_1 + \cos^2 2\theta_1 \cos \delta_{1m}\right) \\
&\quad - 0.5 \sin 2(\beta - \theta_2) \sin \delta_{2n} \cos 2\theta_1 \sin \delta_{1m} \\
M_{14}^{(m,n)} &= 0.5\,[\cos 2\theta_2 \cos 2(\beta - \theta_2) - \sin 2\theta_2 \sin 2(\beta-\theta_2) \cos \delta_{2n}] \\
&\quad \sin 2\theta_1 \sin \delta_{1m} \\
&\quad + 0.5[\sin 2\theta_2 \cos 2(\beta-\theta_2) + \cos 2\theta_2 \sin 2(\beta-\theta_2) \cos \delta_{2n}] \\
&\quad \cos 2\theta_1 \sin \delta_{1m} \\
&\quad + 0.5 \sin 2(\beta - \theta_2) \sin \delta_{2n} \cos \delta_{1m}
\end{aligned} \tag{9}$$

Equation (8) can be simplified as

$$\mathbf{I} = \mathbf{M}_{\mathrm{det}}\mathbf{S} \tag{10}$$

The intensity vector $\mathbf{I}$ is measured by the imaging detector. The modulation matrix $\mathbf{M}_{\mathrm{det}}$ is determined by the optical properties of the BBCs and the thin polarizer, which can be calculated referring to (9) or obtained through system calibration. Finally, the full Stokes vector of the incident light can be calculated by

$$\mathbf{S} = \begin{bmatrix} s_0 \\ s_1 \\ s_2 \\ s_3 \end{bmatrix} = \begin{bmatrix} M_{11}^{(0,0)} & M_{12}^{(0,0)} & M_{13}^{(0,0)} & M_{14}^{(0,0)} \\ M_{11}^{(0,1)} & M_{12}^{(0,1)} & M_{13}^{(0,1)} & M_{14}^{(0,1)} \\ M_{11}^{(1,0)} & M_{12}^{(1,0)} & M_{13}^{(1,0)} & M_{14}^{(1,0)} \\ M_{11}^{(1,1)} & M_{12}^{(1,1)} & M_{13}^{(1,1)} & M_{14}^{(1,1)} \end{bmatrix}^{-1} \begin{bmatrix} I_{00} \\ I_{01} \\ I_{10} \\ I_{11} \end{bmatrix} = \mathbf{M}_{\mathrm{det}}^{-1}\mathbf{I} \tag{11}$$

Equation (11) implies that the Stokes vector of the incident light is calculable when $\mathbf{M}_{\mathrm{det}}$ is invertible matrix (full rank), which can be easily achieved by selecting a proper set of parameters (i.e. β, θ_1, θ_2, δ_{10}, δ_{11}, δ_{20}, and δ_{21}). In fact, there are infinite selections. However, a judicious selection of these seven parameters can significantly minimize the influence of the noise perturbation and systematic error. For a general purpose polarimeter, the polarimetric modulation matrix $\mathbf{M}_{\mathrm{det}}$ should be as far from singular as possible, i.e. it should be well-conditioned. The condition number (CN) is

a good indicator to determine whether the modulation matrix is well-conditioned or not [26], which is expressed as

$$CN = \|\mathbf{M}_{\text{det}}\|_2 \left\|\mathbf{M}_{\text{det}}^{-1}\right\|_2 \tag{12}$$

where $||\cdot||_2$ signify the 2-norm of a matrix.

A useful interpretation of the CN of a matrix is that the reciprocal 1/CN measures how close a matrix is to being singular [27]. And the magnification of error propagation is generally proportional to the CN for a linear system of equations. Our goal in optimizing a Stokes polarimeter is to minimize the CN of $\mathbf{M}_{\text{det}}$, which will minimize the relative errors result from uncertainties in $\mathbf{M}_{\text{det}}$ and $\mathbf{I}$. Thus, one can measure the complete Stokes components referring from Equation (11) according to an image obtained through the proposed polarimeter, and the system parameters can be optimized referring to Equation (12).

III. PARAMETER OPTIMIZATION AND NUMERIC ANALYSIS

Equations (8) and (9) suggest that one can select a number of different polarimeters for polarization imaging by configuring different sets of system parameters (i.e. β, θ_1, θ_2, δ_{10}, δ_{11}, δ_{20}, and δ_{21}). For a general purpose polarimeter, as shown in Equation (12), one should keep the polarimetric measurement matrix as far from singular as possible, i.e. it should be well-conditioned by minimizing the number of CN. In this paper, an optimization algorithm is also build based on the quasi-Newton method to obtain the well-conditioned configuration by minimizing the CN of $\mathbf{M}_{\text{det}}$ similar with optimization studies performed on rotating-retarder Stokes polarimeters [28] and on a liquid-crystal-based Stokes polarimeter [29]. The corresponding optimization processes are also written for optimizing and optimizing the performance of the proposed polarimeter in Matlab environment. Initially, a random set of parameters is substituted into the function. After tens of operations, the function reaches the minimum CN and the optimized parameter set. However, sometimes the function may not reach the global minimum CN value from a random parameter set. So, it is necessary to substitute more sets of random parameters into the function to reach the global minimum CN.

TABLE 1. An optimized parameter set obtained from the optimization function and a random parameter set (Units-°).

Variables	Optimized	Random
θ_1	4.7	47
δ_{10}	230.0	199
δ_{11}	50.0	68
θ_2	107.9	74
δ_{20}	140.8	217
δ_{21}	31.2	38
β	331.8	69
CN	1.7321	14.51

Generally, there are infinite parameter sets for the minimum CN, corresponding to infinite polarimeters with equivalent performance. Table 1 lists one of the well-conditioned configurations. And for comparative analysis, it also lists a random configuration which makes the $\mathbf{M}_{\text{det}}$ invertible.

It is convenient and visualized to present the modulation matrix on a Poincaré sphere. The polarization properties of the four adjacent rectangles of a group are marked on the Poincaré sphere as the vertexes of a tetrahedron. The smaller the CN is, the more regular the tetrahedron gets. Fig. 4 shows two tetrahedrons on the Poincaré sphere of these two polarimeters listed in table 1. The side lengths of the tetrahedrons are (0.121, 2.929, 2.299, 2.854, 2.186, 0.121) (Fig. 4(a)) and (2.667, 2.667, 2.667, 2.667, 2.667, 2.667) (Fig.4(b)) respectively. We can see that the well-conditioned parameter set with minimum CN (1.7321) corresponds to a regular tetrahedron up on the Poincaré sphere. And the random parameter set corresponds to an irregular tetrahedron although the modulation matrix $\mathbf{M}_{\text{det}}$ is invertible.

We also generate 1000 incident lights with different states of polarization (SOPs) to evaluate quantificationally the performance of the proposed polarimeter. As shown in Fig. 5(a) and (b), the SOPs are evenly distributed on the Poincaré sphere, at 20 cross section circles between the north and the south pole. On each circle, 50 SOPs are located

$$\mathbf{M}_P(\beta) = \frac{1}{2}\begin{bmatrix} 1 & \cos 2\beta & \sin 2\beta & 0 \\ \cos 2\beta & \cos^2 2\beta & \sin 2\beta \cos 2\beta & 0 \\ \sin 2\beta & \sin 2\beta \cos 2\beta & \sin^2 2\beta & 0 \\ 0 & 0 & 0 & 0 \end{bmatrix} \tag{3}$$

$$\mathbf{M}_{BBC2}(\theta_2, \delta_{2n}) = \begin{bmatrix} 1 & 0 & 0 & 0 \\ 0 & \cos^2 2\theta_2 + \sin^2 2\theta_2 \cos\delta_{2n} & \sin 2\theta_2 \cos 2\theta_2(1-\cos\delta_{2n}) & -\sin 2\theta_2 \sin\delta_{2n} \\ 0 & \sin 2\theta_2 \cos 2\theta_2(1-\cos\delta_{2n}) & \sin^2 2\theta_2 + \cos^2 2\theta_2 \cos\delta_{2n} & \cos 2\theta_2 \sin\delta_{2n} \\ 0 & \sin 2\theta_2 \sin\delta_{2n} & -\cos 2\theta_2 \sin\delta_{2n} & \cos\delta_{2n} \end{bmatrix} \tag{4}$$

$$\mathbf{M}_{BBC1}(\pi-\theta_1, \delta_{1m}) = \begin{bmatrix} 1 & 0 & 0 & 0 \\ 0 & \cos^2 2\theta_1 + \sin^2 2\theta_1 \cos\delta_{1m} & -\sin 2\theta_1 \cos 2\theta_1(1-\cos\delta_{1m}) & \sin 2\theta_1 \sin\delta_{1m} \\ 0 & -\sin 2\theta_1 \cos 2\theta_1(1-\cos\delta_{1m}) & \sin^2 2\theta_1 + \cos^2 2\theta_1 \cos\delta_{1m} & \cos 2\theta_1 \sin\delta_{1m} \\ 0 & -\sin 2\theta_1 \sin\delta_{1m} & -\cos 2\theta_1 \sin\delta_{1m} & \cos\delta_{1m} \end{bmatrix} \tag{5}$$

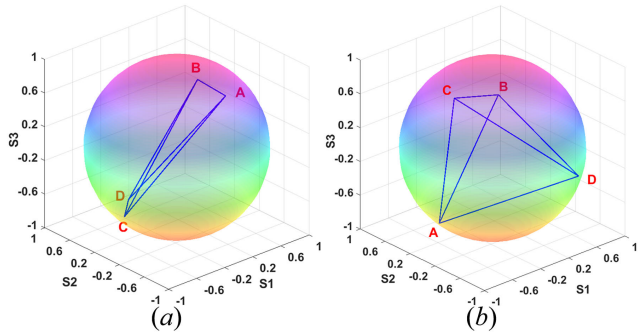

FIGURE 4. The tetrahedrons on the Poincaré sphere of two polarimeters listed in table 1. (a) The polarimeter with random parameter set. (b) The polarimeter with well-conditioned parameter set.

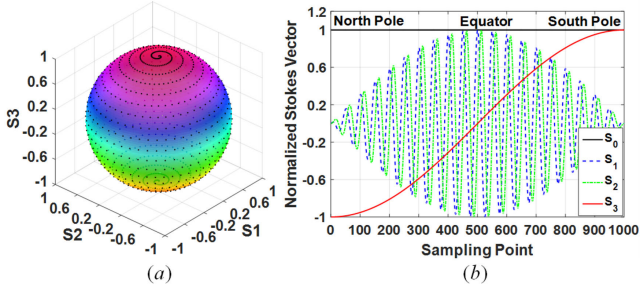

FIGURE 5. The 1000 SOPs of the test lights (a) SOPs shown on the Poincaré sphere. (b) Normalized Stokes vectors of the 1000 test lights.

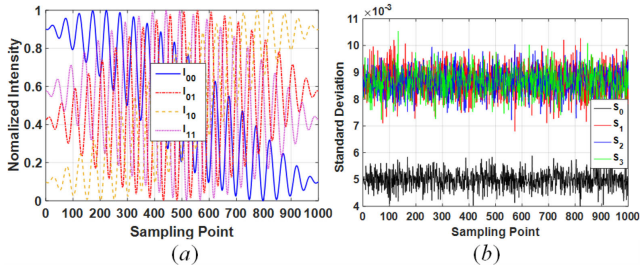

FIGURE 6. Performance of the well-conditioned polarimeter (a) Calculated light intensities for 1000 groups input SOP. (b) The standard deviations of the Stokes vector, caused by the intensity variance of the incident lights.

with equal interval. Substitute the well-conditioned parameter set from table 1 and the SOPs of the incident lights into Equations (8)-(10), 1000 sets of intensity values can be calculated, which are drawn in Fig. 6(a). For each SOP, we add an independent Gaussian noise to the incident light and simulate 100 polarization measuring results. In other word, we test the polarimeter 100 times at each SOP with an incident light that has 1% standard variance of intensity. Fig. 6(b) shows the standard deviations of the measured full Stokes vector components at each SOP, which is about 5×10^{-3} for S_0, and 8.7×10^{-3} for S_1, S_2 and S_3. This is due to systematic error or the error propagation of the well-conditioned polarimeter caused by noise perturbation. Comparatively, the standard deviations of full Stokes components for random parameter set are about 0.031, 0.037, 0.042 and 0.038 respectively under the same condition.

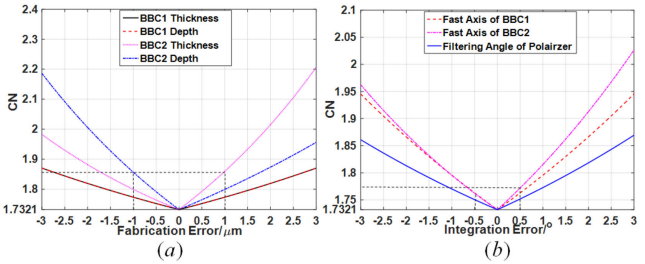

FIGURE 7. Deviations of CN from the well-conditioned configuration when fabrication errors and integration errors are existed. (a). fabrication errors including thickness and depth of BBCs and (b). integration errors.

It indicates that the parameter selection for the proposed polarimeter will influence its performance greatly.

We also make sensitivity analysis for the well-conditioned configuration considering possible fabrication and integration errors for validating the feasibility of the proposed polarimeter. Assuming that quartz material is used to manufacture these two BBCs and the wavelength of incident light is at 632.8nm, the corresponding refractive indexes n_0 and n_e are 1.54264324 and 1.5517112 respectively. The nominal thicknesses (i.e. d_{10} and d_{20}) and the depth of grooves (i.e. d_{11} and d_{21}) are (254μm and 237μm) and (219μm and 215μm) with three additional wavenumbers. Here we give a relax thickness or depth errors ranging from -3μm to $+3\mu$m relative nominal values. The range of integration errors including angle of the fast axes of the BBCs and the filtering angle of the thin polarizer are ranging from $-3°$ to $+3°$. The deviations from the minimal CN due to different fabrication errors and integration errors are drawn in Fig. 7. As seen from Fig. 7(a), the CN increases by a quasi-linear tendency with increasing of thickness and depth errors of the BBCs. And the maximum CN is still under 2.2 when the fabrication errors are up to $\pm 3\mu$m. Comparatively, the CN is more sensitive to the thickness and depth error of BBC2, and the maximum CN is under 1.87 for the same fabrication errors of BBC1. In practical application, the thickness and depth errors can be controlled easily under 1μm, which leads to a maximum CN of 1.86, which is under 7.5% of the theoretical CN. The CN has a more relax requirement for integration errors including angle of the fast axes of the BBCs and the filtering angle of the thin polarizer. And the maximum CN is not over 2.03 when the integration errors is ranging from $-3°$ to $+3°$. It is mature in μm-level fabrication for micro-nano optics. There are three main steps including mask plate design, mask plate fabrication using laser direct writing and birefringent crystal plate etching. In fact, the BBCs and the thin polarizer can be aligned within $\pm 0.5°$ and even $\pm 0.1°$, which leads to a maximum CN of 1.77. Sensitivity analysis show that the CN of the proposed polarimeter is stable under normal fabrication errors and integration errors. Moreover, these errors can be calibrated for more accurate polarization imaging.

Sensitivity analysis results illustrates that small deviations of systematic parameter will not change significantly the CN of the proposed polarimeter, which means a relative relax tolerance for fabrication and integration is required. That will

reduce the cost and complexity of fabrication and integration. Certainly, chromatic aberration always exists in a transmission optics system, which means the proposed polarimeter should work at a limited wavelength coverage. For the given example, the wavelength coverage is from 557nm to 775nm for a relaxing requirement CN of 2.5, which will be narrowed furtherly from 613nm to 652nm when three additional wavenumbers are considered.

IV. SUMMARY AND CONCLUSION

In conclusion, a novel and compact polarimeter is proposed for full-Stokes polarization imaging without using any kinds of micro-polarizer array. Instead of making individual array pixels, the proposed polarimeter adopts two joint pieces of birefringent crystal with perpendicular grooves to achieve four different retardances, which facilitates the fabrication and the integration. Numeric simulation results show that the measurement errors of full Stokes components are all better than 1×10^{-2} when 1% variance of incident light intensity is considered, which indicates the proposed polarimeter has good noise immunity. Besides that, sensitivity analysis results show that the proposed polarimeter has a relative relax requirement for possible errors, which leads to easier fabrication and integration. With the advantages of simultaneity, compactness and easier fabrication, the proposed method is more attractive to a variety of applications. Certainly, this paper mainly focuses on demonstrating a new kind of polarimeter and theoretical proof of its performance by applying the existing and validated fundamental optics and physics laws. We will validate the proposed method by experimental study before developing standard product.

ACKNOWLEDGMENT

The authors would like to thank Prof. Wenhan Jiang and Xuejun Zhang for their helpful discussions and good suggestions. They would also like to thank the reviewers for their constructive comments and useful suggestions, which helped to improve the quality of this paper.

REFERENCES

[1] G. Anna, F. Goudail, and D. Dolfi, "Polarimetric target detection in the presence of spatially fluctuating Mueller matrices," *Opt. Lett.*, vol. 36, no. 23, pp. 4590–4592, 2011.

[2] M. R. Antonelli, A. Pierangelo, T. Novikova, P. Validire, A. Benali, B. Gayet, and A. De Martino, "Mueller matrix imaging of human colon tissue for cancer diagnostics: How Monte Carlo modeling can help in the interpretation of experimental data," *Opt. Express*, vol. 18, no. 10, pp. 10200–10208, 2010.

[3] K. A. Vermeer, F. M. Vos, B. Lo, Q. Zhou, H. G. Lemij, A. M. Vossepoel, and L. J. van Vliet, "Modeling of scanning laser polarimetry images of the human retina for progression detection of glaucoma," *IEEE Trans. Med. Imag.*, vol. 25, no. 5, pp. 517–528, May 2006, doi: 10.1109/TMI.2006.871433.

[4] A. Kimachi, "Polarization imaging for material classification," *Opt. Eng.*, vol. 47, no. 12, Dec. 2008, Art. no. 123201.

[5] G. Dolgos and J. V. Martins, "Polarized Imaging Nephelometer for *in situ* airborne measurements of aerosol light scattering," *Opt. Express*, vol. 22, no. 18, pp. 21972–21990, 2014.

[6] F. A. Iglesias, A. Feller, K. Nagaraju, and S. K. Solanki, "High-resolution, high-sensitivity, ground-based solar spectropolarimetry with a new fast imaging polarimeter," *Astron. Astrophys.*, vol. 590, p. A89, Jun. 2016.

[7] J. S. Tyo, D. L. Goldstein, D. B. Chenault, and J. A. Shaw, "Review of passive imaging polarimetry for remote sensing applications," *Appl. Opt.*, vol. 45, no. 22, pp. 5453–5469, Aug. 2006.

[8] J. E. Ahmad and Y. Takakura, "Error analysis for rotating active Stokes-Mueller imaging polarimeters," *Opt. Lett.*, vol. 31, no. 19, pp. 2858–2860, Oct. 2006.

[9] S. Alali, T. Yang, and I. A. Vitkin, "Rapid time-gated polarimetric Stokes imaging using photoelastic modulators," *Opt. Lett.*, vol. 38, no. 16, pp. 2997–3000, Aug. 2013.

[10] Y. Chang, Y.-L. Lo, and Q.-H. Phan, "Full-field Stokes–Mueller matrix imaging polarimetry system based on electro-optical modulators," *IEEE Photon. J.*, vol. 10, no. 6, Nov. 2018, Art. no. 6602507, doi: 10.1109/JPHOT.2018.2880221.

[11] J. Guo, D. Ren, C. Liu, Y. Zhu, J. Dou, X. Zhang, and C. Beck, "Design and calibration of a high-sensitivity and high-accuracy polarimeter based on liquid crystal variable retarders," *Res. Astron. Astrophys.*, vol. 17, no. 1, pp. 87–96, 2017.

[12] Z. Ding, Y. Yao, X. S. Yao, X. Chen, C. Wang, S. Wang, and T. Liu, "Demonstration of compact *in situ* Mueller-matrix polarimetry based on binary polarization rotators," *IEEE Access*, vol. 7, pp. 144561–144571, 2019, doi: 10.1109/ACCESS.2019.2945812.

[13] R. M. A. Azzam, "Arrangement of four photodetectors for measuring the state of polarization of light," *Opt. Lett.*, vol. 10, no. 7, pp. 309–311, Jul. 1985.

[14] T. Mu, C. Zhang, Q. Li, and R. Liang, "Error analysis of single-snapshot full-Stokes division-of-aperture imaging polarimeters," *Opt. Express*, vol. 23, no. 8, pp. 10822–10835, Apr. 2015.

[15] T. York and V. Gruev, "Characterization of a visible spectrum division-of-focal-plane polarimeter," *Appl. Opt.*, vol. 51, no. 22, pp. 5392–5400, Aug. 2012.

[16] N. Gu, B. Yao, L. Huang, and C. Rao, "Design and analysis of a novel compact and simultaneous polarimeter for complete Stokes polarization imaging with a piece of encoded birefringent crystal and a micropolarizer array," *IEEE Photon. J.*, vol. 10, no. 2, Apr. 2018, Art. no. 6801312, doi: 10.1109/JPHOT.2018.2802908.

[17] A. Ahmed, X. Zhao, J. Chang, H. Ma, V. Gruev, and A. Bermak, "Four-directional adaptive residual interpolation technique for DoFP polarimeters with different micro-polarizer patterns," *IEEE Sensors J.*, vol. 18, no. 19, pp. 7990–7997, Oct. 2018, doi: 10.1109/JSEN.2018.2861825.

[18] M. Kulkarni and V. Gruev, "Integrated spectral-polarization imaging sensor with aluminum nanowire polarization filters," *Opt. Express*, vol. 20, no. 21, pp. 22997–23012, Oct. 2012.

[19] V. Gruev, A. Ortu, N. Lazarus, J. V. D. Spiegel, and N. Engheta, "Fabrication of a dual-tier thin film micropolarization array," *Opt. Express*, vol. 15, no. 8, pp. 4994–5007, Apr. 2007.

[20] W.-L. Hsu, J. Ma, G. Myhre, K. Balakrishnan, and S. Pau, "Patterned cholesteric liquid crystal polymer film," *J. Opt. Soc. Amer. A, Opt. Image Sci.*, vol. 30, no. 2, pp. 252–258, Feb. 2013.

[21] X. Zhao, A. Bermak, F. Boussaid, and V. G. Chigrinov, "Liquid-crystal micropolarimeter array for full Stokes polarization imaging in visible spectrum," *Opt. Express*, vol. 18, no. 17, pp. 17776–17787, Aug. 2010.

[22] G. Myhre, W.-L. Hsu, A. Peinado, C. LaCasse, N. Brock, R. A. Chipman, and S. Pau, "Liquid crystal polymer full-Stokes division of focal plane polarimeter," *Opt. Express*, vol. 20, no. 25, pp. 27393–27409, Dec. 2012.

[23] W.-L. Hsu, G. Myhre, K. Balakrishnan, N. Brock, M. Ibn-Elhaj, and S. Pau, "Full-Stokes imaging polarimeter using an array of elliptical polarizer," *Opt. Express*, vol. 22, no. 3, pp. 3063–3074, Feb. 2014.

[24] C. Xu, C. Ke, J. Ma, Y. Huang, and Z. Zeng, "Full-Stokes polarization imaging method based on the self-organized grating array in fused silica," *Sci. Rep.*, vol. 8, p. 2331, Feb. 2018.

[25] C. Xu, J. Ma, C. Ke, Y. Huang, Z. Zeng, and W. Weng, "Numerical study of a DoFP polarimeter based on the self-organized nanograting array," *Opt. Express*, vol. 26, no. 3, pp. 2517—-2527, Feb. 2018.

[26] A. Peinado, A. Lizana, J. Vidal, C. Iemmi, and J. Campos, "Optimization and performance criteria of a Stokes polarimeter based on two variable retarders," *Opt. Express*, vol. 18, no. 10, pp. 9815–9830, May 2010.

[27] M. H. Smith, "Optimization of a dual-rotating-retarder Mueller matrix polarimeter," *Appl. Opt.*, vol. 41, no. 13, pp. 2488–2493, May 2002.

[28] D. S. Sabatke, M. R. Descour, E. L. Dereniak, W. C. Sweatt, S. A. Kemme, and G. S. Phipps, "Optimization of retardance for a complete Stokes polarimeter," *Opt. Lett.*, vol. 25, no. 11, pp. 802–804, Jun. 2000.

[29] J. S. Tyo, "Noise equalization in Stokes parameter images obtained by use of variable-retardance polarimeters," *Opt. Lett.*, vol. 25, no. 16, pp. 1198–1200, Aug. 2000.

NAITING GU was born in Huaiyuan County, Bengbu, Anhui, China, in 1985. He received the B.S. degree in opto-electric information engineering from Chongqing University, Chongqing, in 2007, and the Ph.D. degree in optical engineering from the University of Chinese Academy of Sciences, Beijing, in 2012.

From 2011 to 2014, he was a Research Assistant with the Key Laboratory on Adaptive Optics, Chinese Academy of Sciences, where he has been an Associate Professor and a Professor, since 2015. He is the author of two books, more than 30 articles, and more than 20 inventions. His research interests include compact polarimeter, interferometry, large optical telescope, adaptive optics, and the relative applications.

DUO XU was born in Xingping County, Xianyang, Shanxi, China, in 1994. He received the B.S. degree in optoelectronic information science and engineering from China Jiliang University, Hangzhou, in 2017. He is currently pursuing the master's degree with the University of Electronic Science and Technology of China. His main research interests include compact polarimeter and polarimetry.

LINHAI HUANG was born in Shanwei, Guangdong, China, in 1980. He received the B.S. and M.S. degrees in physics and telecommunication engineering from South China Normal University, Guangzhou, in 2003, and the Ph.D. degree in optical engineering from the University of Chinese Academy of Sciences, Beijing, in 2009.

From 2009 to 2011, he was a Research Assistant with the Key Laboratory on Adaptive Optics, Chinese Academy of Sciences, where he has been an Associate Professor and a Professor, since 2012. He is the author of more than 30 articles and more than 15 inventions. His research interests include adaptive optics, optical imaging, target tracking, and the relative applications.

CHANGHUI RAO was born in Shangrao, Jiangxi, China, in 1971. He received the B.S. degree in electronic instrument and testing technique from Wuhan University, Wuhan, in 1993, and the M.S. and Ph.D. degrees in optical engineering from the University of Chinese Academy of Sciences, Beijing, in 1997 and 2001, respectively.

From 1993 to 2004, he was a Research Assistant with the Key Laboratory on Adaptive Optics, Chinese Academy of Sciences, where he has been an Associate Professor and a Professor, since 2005. He is the author of three books, more than 200 articles, and more than 100 inventions. His research interests include adaptive optics, solar telescope, and the post focus instruments.